Photochemical & Photobiological Sciences (2025) 24:1–12
https://doi.org/10.1007/s43630-024-00663-x

ORIGINAL PAPERS

Type I and Type II photosensitization of DNA etheno adducts

Paloma Lizondo-Aranda[1] · Gemma M. Rodríguez-Muñiz[1] · Miguel A. Miranda[1] · Belinda Heyne[2] · Virginie Lhiaubet-Vallet[1]

Received: 27 September 2024 / Accepted: 13 November 2024 / Published online: 19 December 2024
© The Author(s) 2024

Abstract

Photophysical and photochemical studies were carried out to examine the photoreactivity of etheno adducts, 1,N^6-ethenoadenine (εdA) and 1,N^2-ethenoguanine (εdG), in the presence of two well-known photosensitizers acting by Type I and/or Type II mechanisms such as 4-carboxybenzophenone (CBP) and rose Bengal (RB), respectively. Steady-state photolysis experiments combined with HPLC and mass spectroscopy measurements lead to photoproducts that correspond to the repaired nucleosides. To determine the mechanism of this photooxidation processes, phosphorescence spectroscopy, direct detection of singlet oxygen luminescence and laser flash photolysis were carried out. This work establishes that εdG and εdA are sensitive to both types of processes (Type I and II).

Graphical abstract

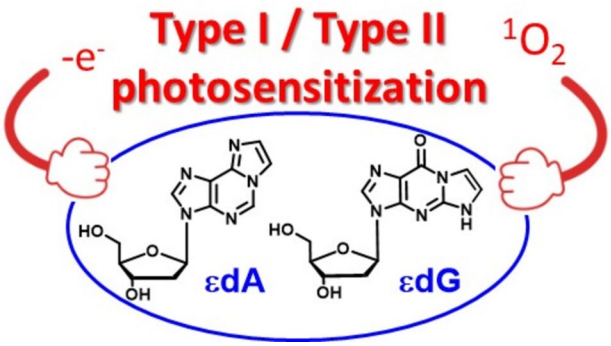

Keywords Singlet oxygen · DNA lesions · Electron transfer · Lipid peroxidation

1 Introduction

Photosensitization of DNA bases has attracted considerable interest to understand the interaction between light and nucleic acids and its role in the appearance of harmful effects such as photoaging, phototoxicity, photocarcinogenesis, etc. [1]. Over the years, a multitude of photosensitizers have been reported to generate DNA lesions through three main types of mechanisms corresponding to Type I and/or Type II processes, or triplet–triplet energy transfer (TTET) [2, 3]. One of the most sensitive nucleobases to oxidation through Type I and Type II processes is 2′-deoxyguanosine (dG) forming 8-oxo-7,8-dihydroguanosine (8-oxoG) [4, 5]. The 8-oxoG is described to be a primary photolesion from

✉ Belinda Heyne
bjmheyne@ucalgary.ca

✉ Virginie Lhiaubet-Vallet
lvirgini@itq.upv.es

[1] Instituto Universitario Mixto de Tecnología Química (UPV-CSIC), Universitat Politècnica de València, Consejo Superior de Investigaciones Científicas, Avda de los Naranjos s/n, 46022 Valencia, Spain

[2] Department of Chemistry, University of Calgary, 2500 University Drive NW, Calgary, AB T2N 1N4, Canada

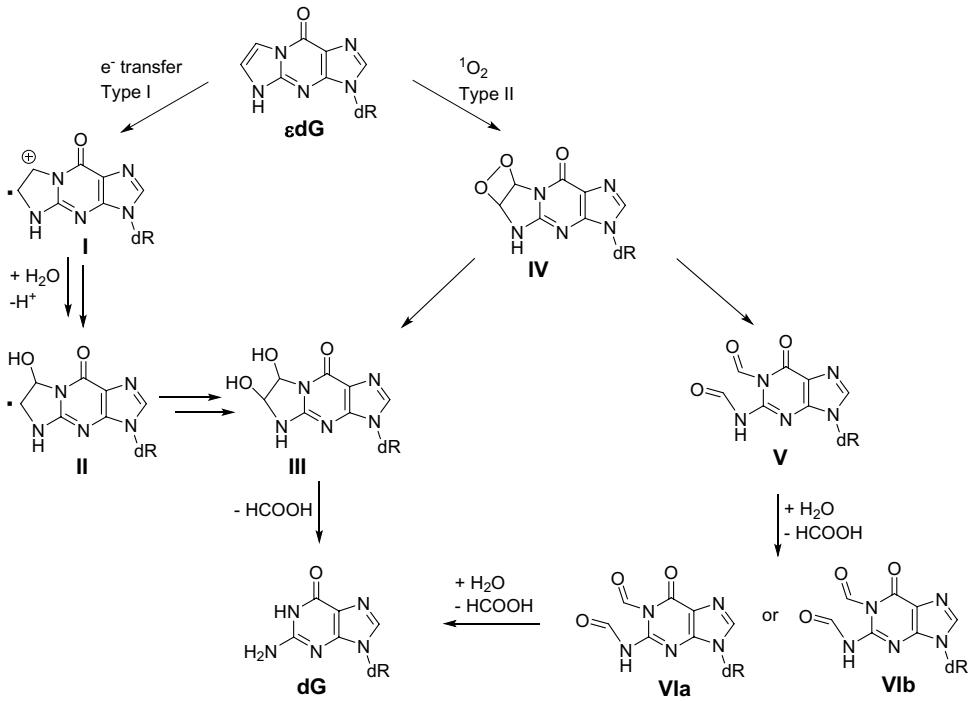

Scheme 1 Proposed mechanism for Type I and Type II (adapted from reference [17]) photosensitized degradation of εdG

the canonical nucleobase; however, its photosensitized degradation leads to the formation of secondary photoproducts with mutagenic properties such as 2,2-diamino-oxazolone (Ox) [6], spiroiminodihydantoin (Sp) or guanidinohydantoin (Gh) [7]. As in the case of 8-oxoG, DNA (photo)lesions are not necessarily photostable and might suffer further photodegradation. With this in mind, DNA etheno adducts (*ε-adducts)* warrant further study as interesting lesions for investigating their photoreactivity.

DNA *ε-adducts* come from endogenous reactions involving metabolically generated aldehydes derived from lipid peroxidation [8, 9] or human carcinogen metabolites such as vinyl chloride [10]. As a consequence, they represent a background DNA damage in rodent or human tissues [11, 12]. These adducts contain a five-membered ring formed between the exocyclic amine and a nitrogen atom of the purine or pyrimidine core. A total of four *ε-adducts* have been identified in DNA; they correspond to 1,N^6-ethenoadenine, 3,N^4-ethenocytosine, 1,N^2-ethenoguanine and N^2,3-ethenoguanine. Remarkably, these ubiquitous lesions are not innocuous and exhibit highly mutagenic properties inducing base transitions or transversion in mammal cells [8, 13]. In addition, we recently reported the photophysics of εdC and εdG using a combined experimental and theoretical study [14, 15], and showed that addition of the extra etheno ring on 2′-deoxycytosine (dC) or dG alters their photobehavior and results in an increase of the lifetime and quantum yield of fluorescence. These findings could be associated with a higher photoreactivity of the lesion compared to the canonical nucleobase. Interestingly, the computational results for εdG also point to a lower oxidation potential of this nucleobase compared with that of dG [14].

As a matter of fact, the chemical stability of 1,N^2-etheno-2′-deoxyguanosine (εdG) has been tackled in the literature to evaluate the accuracy of the analytical methods employed in its quantification as an oxidative stress biomarker [16]. Thus, its degradation by hydrolysis under acidic conditions (pH 2), Fenton reaction, or one-electron oxidation by $SO_4^{\bullet-}$ has been documented [16], ultimately resulting in the repaired nucleotide, dG, for the latter two processes. Furthermore, the reactivity of three *ε-adducts* 1,N^6-etheno-2′-deoxyadenine (εdA), 3,N^4-etheno-2′-deoxycytosine (εdC) and εdG with $^1O_2$ has been studied few years ago [17]. Bimolecular rate constants ranging from 2.3 to 4.4×10^6 $M^{-1}s^{-1}$ have been determined for $^1O_2$ quenching. It is noteworthy that these values are close to that measured for quenching by 2′-deoxyguanosine (dG) of ca. 5.4×10^6 $M^{-1}s^{-1}$ [17], which is the only canonical nucleoside able to chemically react with this reactive oxygen species. In addition, thermally generated $^1O_2$ from naphthalene-derived endoperoxides was shown to attack εdG to yield the original nucleoside dG after formation of an oxetane intermediate (Scheme 1, Type II route). Deactivation of $^1O_2$ by the other two *ε-adducts* was, by contrast, interpreted as a physical quenching [17].

Here, we addressed the study of the processes involved in the photoreactivity of two *ε-adducts* derived from purines, εdG and εdA, using rose Bengal (RB^{2-}) and 4-carboxybenzophenone (CBP) as Type II and/or I photosensitizers, respectively (Fig. 1). On the one hand, RB^{2-} is a well-known photosensitizer that has been widely used due to its high

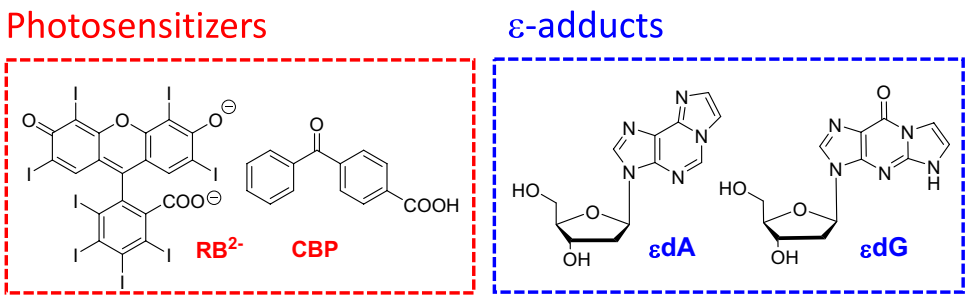

Fig. 1 Structure of the *ε-adducts* under study, rose Bengal (RB^{2-}) and 4-carboxybenzophenone (CBP)

quantum yield of $^1O_2$ formation ($\Phi_\Delta = 0.76$ in water) [18]. As a consequence, its mode of action has been mostly attributed to a Type II mechanism that corresponds to a reaction between the substrate and $^1O_2$. RB^{2-} has been, for example, employed to investigate the photoproducts obtained from $^1O_2$ attack on nucleoside or DNA molecules, leading to the formation of 8-oxoG, Ox, Sp or Gh [4, 5]. However, it has also been shown that RB^{2-} could undergo oxidative and reductive triplet excited state quenching in biological media [19], which suggests that under particular conditions Type I processes can take place and compete with the $^1O_2$-derived mechanism. On the other hand, benzophenone and its derivatives such as CBP have been described as classical and paradigmatic chromophores [20]. They are well-established DNA photosensitizers able to yield a large variety of lesions arising from Type I (electron transfer and hydrogen abstraction) or Type II processes, but also from triplet–triplet energy transfer (TTET) to thymine, the nucleobase with the lowest triplet excited state energy [21]. In this work, CBP is used as a water-soluble derivative, and *ε-adducts* photosensitization was run under anaerobic conditions to prevent Type II mechanism and focus attention on a Type I process.

2 Results

2.1 Photosensitization of ε-adducts by RB^{2-}

The *ε-adducts* reactivity toward $^1O_2$ was first considered using rose Bengal (RB^{2-}) as a typical Type II photosensitizer [18, 19]. Steady-state photolysis was run for aerated water solutions of the *ε-adducts* (20 μM) and RB^{2-} (10 μM) using white light (emission between 350 and 700 nm) to ensure the excitation of RB^{2-} at its 550 nm absorption band without direct excitation of the *ε-adducts* (Fig. S1). The kinetics of the lesion consumption and photoproducts formation were followed by HPLC. Control experiments were performed by irradiating the lesion alone; expectedly, no changes were observed by HPLC confirming their photostability under our experimental conditions (Fig. S2). Conversely, steady-state photolysis of the *ε-adducts* in the presence of RB^{2-} showed that the initial peak decreases as a function of irradiation time (Figs. 2 and 3, black lines).

The guanine-derived adduct, εdG (eluting at 15 min), exhibited a reactivity similar to that previously reported in the literature [17] as its consumption gave rise to the formation of different products with retention times (t_R) of 5.2–5.4, 6.2, and 10.7 min (Fig. 2). Compound eluting at 6.2 min was assigned to the original nucleobase, dG, by comparison with an authentic sample. Compounds at 5.2–5.4 and 10.7 min were identified by HPLC–MS (Fig. S3) on the basis of Martinez et al. studies [17]. The fast eluting compound with *m/z*

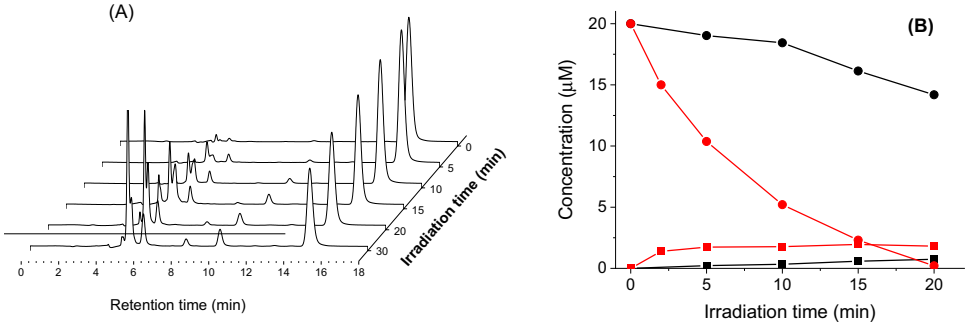

Fig. 2 **a** HPLC chromatograms registered at 260 nm for an aerated solution of 20 μM εdG in the presence of 10 μM RB upon irradiation at different times in H_2O. **B** Variation of the concentration of damaged (εdG, circle) and repaired nucleoside (dG, square) as a function of the irradiation time in H_2O (black) and D_2O (red)

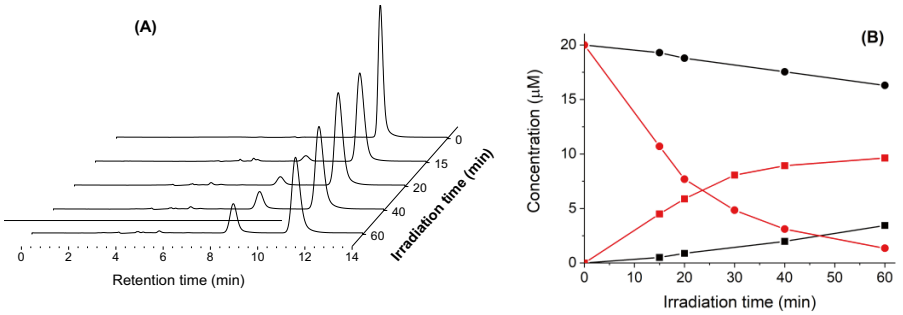

Fig. 3 **a** HPLC chromatograms registered at 260 nm for an aerated solution of 20 μM εdA in the presence of 10 μM RB upon irradiation at different times in H_2O. **B** Variation of the concentration of damaged (εdA, circle) and repaired nucleoside (dA, square) as a function of the irradiation time in H_2O (black) and D_2O (red)

of 326 corresponds to intermediate III, whereas at $t_R = 10.7$ min the registered *m/z* of 296 agrees with the generation of intermediate VIa and/or VIb (Scheme 1).

Interestingly, εdG is not the only ε-adduct that reacted under our experimental conditions. As shown in Fig. 3, εdA (eluting at 11.2 min) was also consumed, but led to the formation of one single product eluting at t_R of ca. 8.5 min and assigned to dA by comparison with an authentic sample and HPLC–MS analysis. In that case, no intermediates of the reaction were detected.

To confirm the role of $^1O_2$ in the degradation of the *ε-adducts* and regeneration of the original DNA bases, irradiations were run in D_2O, where $^1O_2$ lifetime is much longer than in H_2O (ca. 60 vs 4 μs) [22]. Accordingly, the kinetics were faster, reaching an almost complete consumption after 20 and 60 min for εdG and εdA, respectively (Figs. 2B and 3B, red lines).

Thus, RB^{2-} photosensitization of both *ε-adducts* under aerobic conditions leads back to the original nucleosides and provides a photorepair process of these lesions. Recovery of the nucleosides appears to occur in high yields for εdA in D_2O (Fig. 3B). By contrast, dG formation yield reaches less than 10% just after 15 min of irradiation in D_2O. This low yield can be explained not only by the presence of intermediates that, as shown by Martinez et al., slowly evolve to dG, but also by the particular reactivity of dG with $^1O_2$, as it is the only DNA nucleobase able to react with this reactive oxygen species to yield secondary products [23].

2.2 Photophysical study of RB^{2-} in the presence of ε-adducts

Next, the interaction of the *ε-adducts* with $^1O_2$ was studied using time-resolved phosphorescence. Experiments were run recording $^1O_2(^1\Delta g)$ characteristic emission at 1270 nm after excitation at 532 nm of D_2O solutions of RB^{2-} at a concentration of 5 μM ($A_{532} = 0.18$). The initial lifetime τ_0 of ca. 66 μs determined for $^1O_2$ emission was shortened after the addition of increasing amounts of the etheno derivatives (Fig. 4). The $^1O_2$ quenching rate constants ($k_q(^1O_2)$-ε in $M^{-1}s^{-1}$) were

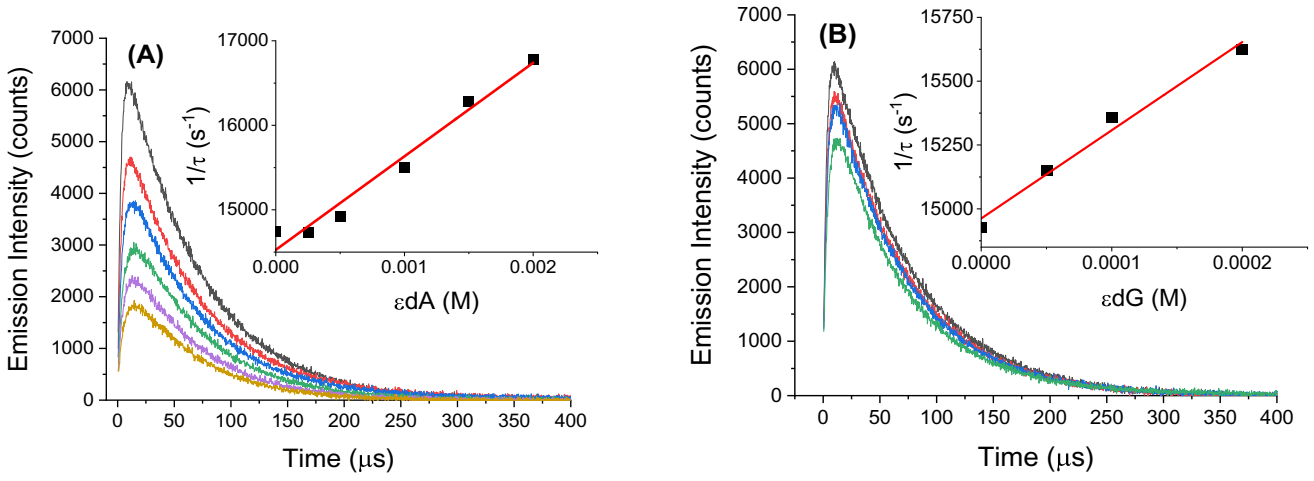

Fig. 4 Time-resolved $^1O_2$ phosphorescence signal ($\lambda_{exc} = 532$ nm, $\lambda_{em} = 1270$ nm) and their corresponding Stern–Volmer plot (insets) obtained from aerated D_2O solutions of 5 μM RB in the presence of increasing amounts of *ε-adducts* (**A**) from 0 to 2 mM for εdA and (**B**) from 0 to 0.2 mM in case of εdG

determined from the Stern–Volmer plots applying the following equation:

$$1/\tau = 1/\tau_0 + k_q\left({}^1O_2\right) - \varepsilon \times [\varepsilon \text{ - adduct}],$$

where τ_0 and τ are the $^1O_2$ lifetime (in s) in the absence and in the presence of a concentration [ε-adduct] of the quencher (in M). Similar values were obtained for the two adducts with $k_q(^1O_2)$-ε in the order of 10^6 $M^{-1}s^{-1}$ (Table 1).

Moreover, a decrease of the top emission intensity was observed for all the additions, which was especially pronounced for εdA (Fig. 4A) where the final adduct concentration was higher (εdG is not soluble at concentration higher than 0.4 mM). This decrease in $^1O_2$ signal intensity could be the result of a lower formation yield of the $^1O_2$ precursor, i.e., RB^{2-} triplet excited state ($^3RB^{2-}$*), as the concentration of the quencher increases. These changes in $^3RB^{2-}$* population can be, indeed, due to several processes.

First, the screening effect resulting from absorption of the etheno derivatives can be discarded due to their lack of absorption at the excitation wavelength (λ_{exc} = 532 nm). Another option is an interaction of the *ε-adducts* with the singlet excited state of the photosensitizer ($^1RB^{2-}$*), which would decrease the excited molecules available for intersystem crossing and population of $^3RB^{2-}$*, resulting in less $^1O_2$ production. To investigate this possibility, steady-state fluorescence experiments were carried out under the same conditions as those of $^1O_2$ detection, but no significant decrease of $^1RB^{2-}$* emission intensity was observed (Fig. S4). Therefore, on the basis of the steady-state fluorescence results, the decrease in the top emission intensity observed in Fig. 4 is not due to a quenching of $^1RB^{2-}$*. Another explanation could rely on the photodegradation of the RB^{2-} during the measurements (each trace is obtained after an accumulation time of 3 min). However, no significant changes were observed when comparing the UV–Vis absorption spectra of the solutions before and after the $^1O_2$ measurement.

A direct interaction between the triplet excited state of RB^{2-} and the *ε-adducts* represents another possibility. Indeed, upon excitation, formation of the triplet manifold is the main route of $^1RB^{2-}$* deactivation with an efficient intersystem crossing, ϕ_{ISC} of ca. 0.8, and thus the reactivity of this state directly with the lesions can play an important role in the photochemical processes [19, 24, 25]. In this context, phosphorescence experiments were performed using RB^{2-} solutions (5 µM) prepared in deuterated water and flushed with N_2 just before the measurements. The phosphorescence emission was registered at room temperature after excitation at 532 nm and showed a maximum at 730 nm with a lifetime τ_0 of ca. 210 µs. Decays were recorded in the presence of increasing amounts of the *ε-adducts* (Fig. 5), and the bimolecular quenching rate constants $k_q(^3RB^{2-}*)$P-ε, summarized in Table 1, were obtained from the Stern–Volmer plots (Fig. 5, insets). These phosphorescence experiments showed that $^3RB^{2-}$* is quenched by εdA and εdG, with a constant two orders of magnitude higher for the latter. Interestingly, for εdG, the quenching rate constant of $^3RB^{2-}$* is also two orders of magnitude higher than that of $^1O_2$.

On these bases, laser flash photolysis experiments were carried out to get more insight into the quenching mechanism and to investigate the presence of other intermediates

Table 1 Quenching rate constants of $^1O_2$, generated after RB^{2-} excitation, by *ε-adducts* ($k_q(^1O_2)$-ε), bimolecular quenching rate constants of $^3RB^{2-}$* by *ε-adducts* determined from phosphorescence, ($k_q(^3RB^{2-}*)$P-ε) and from laser flash photolysis ($k_q(^3RB^{2-}*)$LFP-ε) experiments, and bimolecular quenching rate constants of ^{3}CBP* by *ε-adducts* determined from laser flash photolysis ($k_q(^3CBP*)$LFP-ε) experiments

	$k_q(^1O_2)$-ε ($M^{-1}s^{-1}$)	$k_q(^3RB^{2-}*)$P-ε	$k_q(^3RB^{2-}*)$LFP-ε	$k_q(^3CBP*)$LFP-ε
εdA	9.2×10^5	1.5×10^6	3.8×10^6	2.2×10^9
εdG	3.6×10^6	1.3×10^8	8.5×10^7	3.6×10^9

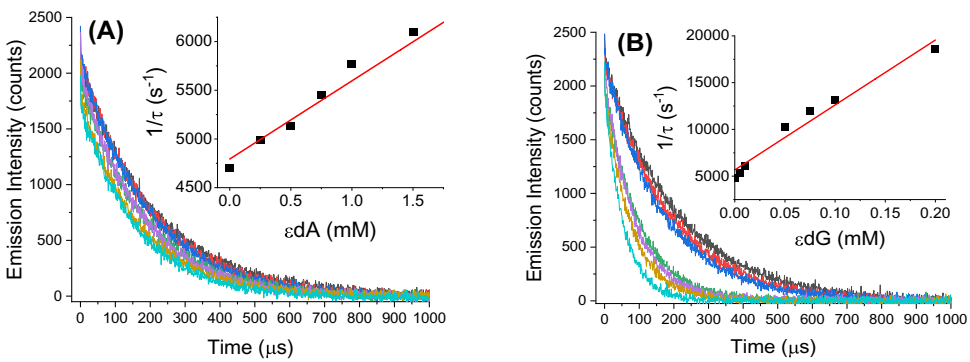

Fig. 5 Time-resolved $^3RB^{2-}$* phosphorescence signals monitored at 690 nm in N_2 obtained from 5 µM RB^{2-} in the presence of increasing amounts of *ε- adducts*: **A** εdA and **B** εdG (from 0 to 2 mM and 0 to 0.2 mM in the case of εdG). Insets: corresponding Stern–Volmer plot

such as radical species in the *ε-adducts* photosensitization process. A previous work revealed that 532 nm laser excitation of RB^{2-} leads not only to the formation of its triplet excited state, but also to oxidative and reductive processes leading to the corresponding ion radicals (Fig. S4) [18]. Thus, experiments were performed by means of a nanosecond pulsed laser (Nd:YAG) using 532 nm as the excitation wavelength. The transient absorption spectra of a degassed solution of RB^{2-} in D_2O at different times after the laser pulse are in agreement with those described in the literature for RB^{2-} [18], and provide evidence for the formation of three transient species (Fig. S4). The first one, exhibiting three maxima at λ_{abs}^{max} 380, 465 and 590 nm, is attributed to the triplet–triplet transition $^3RB^{2-*}$ that starts to decay just after the pulse has a lifetime of $\tau(^3RB^{2-*}) = 82$ µs. The other two transients are longer-lived than $^3RB^{2-*}$ and appear at λ_{abs}^{max} 420 and 460 nm with a relative delay after the pulse. On the basis of literature data, they were assigned to the oxidized ($RB^{\bullet-}$) and reduced ($RB^{\bullet 3-}$) forms.

The typical RB^{2-} signals were obtained in the presence of both *ε-adducts* (Fig. 6), and quenching experiments were run by adding increasing amounts of the different etheno derivatives. For the three lesions, the signal at ca. 600 nm assigned to the triplet–triplet transition was monitored, and bimolecular quenching rate constants of the same order of magnitude as those obtained during the luminescence studies were determined. The obtained values are $k_q(^3RB^{2-*})$ LFP-ε of ca. 3.8×10^6 and 8.5×10^7 $M^{-1}s^{-1}$ for εdA and εdG, respectively (Table 1). Interesting outcomes can be drawn from the ion radical signals. As shown in Fig. 6, when εdA and εdG were added to the RB^{2-} solution, the signals at 380, 465 and 590 nm decay, whereas the transient absorption corresponding to the photosensitizer reduced form $RB^{\bullet 3-}$ at 420 nm remains stable. For further assignment, formation of $RB^{\bullet 3-}$ was forced by adding 1,4-diazabicyclo[2.2.2]octane (DABCO) to the system. Figure S6 shows the transient absorption spectra of RB^{2-} in the presence of 5 mM DABCO, where the $RB^{\bullet 3-}$ signal at 420 nm is clearly observed. Therefore, detection of this species when εdG and εdA are present in the solution, together with $^3RB^{2-*}$ quenching by these *ε-adducts*, points toward a photoredox process where $^3RB^{2-*}$ oxidizes the lesions to yield the photosensitizer reduced form, $RB^{\bullet 3-}$, and the cation radical of the lesions. This latter was not detected in our experiment; however, it could be masked by the band derived from RB^{2-}, have a low molar absorption coefficient or absorb in a region different from the analysis window.

2.3 Photosensitization of ε-adducts by CBP

In view to study a potential electron transfer process leading to *ε-adducts* oxidation, 4-carboxybenzophenone (CBP) was considered as a Type I photosensitizer. First of all, steady-state photolysis experiments were done to investigate the occurrence of the repair process. The *ε-adducts* were irradiated with UVA light in the presence and absence of CBP in deaerated water. Experiments were performed in the absence of oxygen to avoid formation of $^1O_2$ and focus attention on a potential electron transfer process. No degradation of the etheno derivatives occurred during the control irradiation in the absence of CBP. By contrast, in the presence of CBP, photodegradation took place for the two etheno derivatives (Fig. 7). For εdG, the same pattern as that in Fig. 2A was observed in the chromatograms, where the repaired nucleoside was observed together with other peaks at a t_R of ca. 5.2–5.4 and 10.8 min (Fig. 7A). By contrast for εdA, in addition to dA, other photoproducts were formed at short elution times, between 3 and 5 min (Fig. 7B). Due to the low concentration of these compounds, no clear information on their nature was obtained from HPLC–MS analysis.

These results point toward the possibility of a photoinduced anaerobic oxidation process for the purine

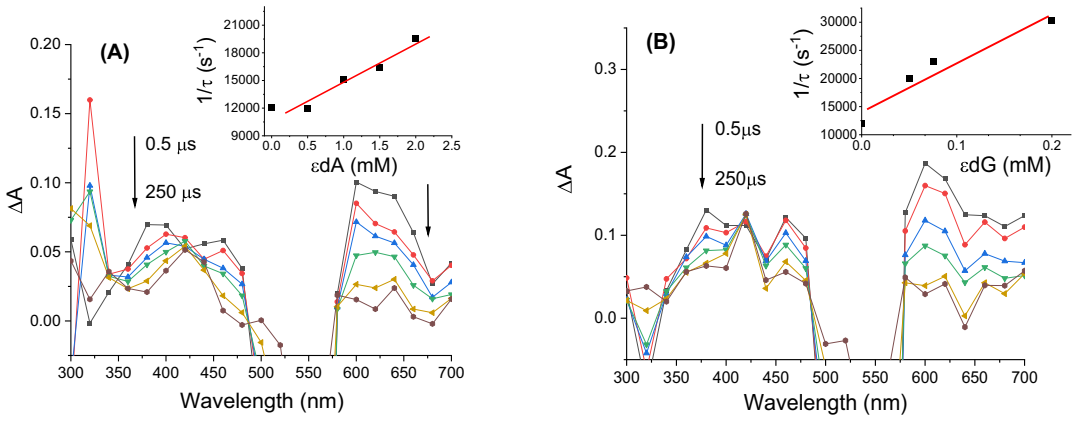

Fig. 6 Transient absorption spectra of a deaerated solution of RB^{2-} in deuterated water after 532 nm excitation in the presence of 2 mM of εdA (**A**) and 0.2 mM of εdG (**B**). Insets: Stern–Volmer plot obtained from decays at 600 nm

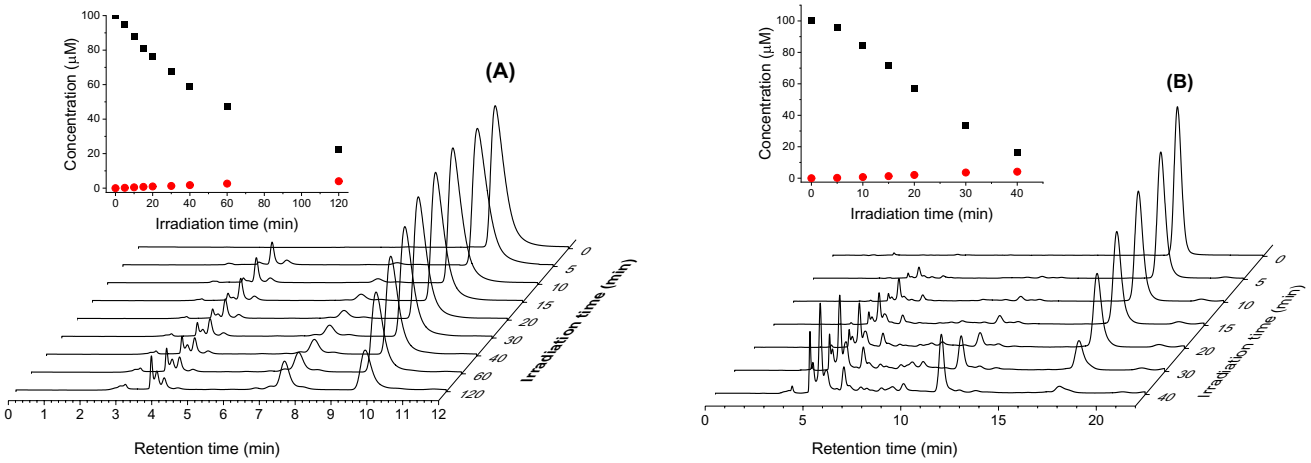

Fig. 7 HPLC chromatograms registered at 260 nm for an anaerobic H_2O solution (1.5% acetonitrile) of **A** εdA or **B** εdG (100 μM) in the presence of CBP (50 μM) upon UVA irradiation at different times. Inset: variation of the concentration of ε-adduct (black square) and repaired nucleoside (red circle) with irradiation time

derivatives, which regenerates the original nucleobase from the *ε-adducts* without intervention of oxygen. In that case, and by contrast with Type II photosensitization, once formed both dA and dG are sensitive to electron transfer, which can lead to the formation of oxidatively generated photoproducts.

2.4 Photophysical study of CBP in the presence of ε-adducts

Laser flash photolysis experiments were carried out at 355 nm to investigate the nature of the observed reactivity. The transient absorption spectra of a N_2 flushed CBP aqueous solution showed two signals at 340 and 560 nm assigned to the CBP triplet excited state (^{3}CBP*) bands by comparison with reported data (Fig. S7) [20]. In the presence of purine-derived *ε-adducts*, the ^{3}CBP* disappeared at short delays after the laser pulse and gave rise to a longer-lived and red-shifted signal with maximum at ca. 580 nm (Fig. 8). This behavior was more pronounced in the case of εdG than for εdA. The new transient was attributed to the ketyl radical of CBP obtained from photoreduction of the ^{3}CBP* and oxidation of the lesions. In this process, the formed anion radical $CBP^{\bullet-}$ is subsequently protonated (Scheme S2) [26] yielding $CBPH^{\bullet}$. This transient radical was further assigned by comparison with the signals obtained for CBP aqueous solution containing 20% of ethanol (inset Fig. S7). In this case, the typical H-abstraction from the solvent led to efficient formation of CBP ketyl radical centered at 580 nm.

Concerning the kinetics, the ^{3}CBP* lifetime was shortened in the presence of the two etheno derivatives. The bimolecular quenching rate constants $k_q(^3\text{CBP*})$-ε obtained from the Stern–Volmer plots were of ca. 3.6×10^9 $M^{-1}s^{-1}$ for εdG and 2.2×10^9 $M^{-1}s^{-1}$ for εdA (Table 1). Interestingly, the $k_q(^3\text{CBP*})$-ε was higher in the case of εdG, which suggests, as reported for the canonical base, a lower oxidation potential of the guanosine derivative with respect to εdA. Altogether, these data are consistent with quenching occurring via electron transfer from the ε-adduct to CBP triplet manifold, and it is further supported by the clear detection of $CBPH^{\bullet}$ in Fig. 8.

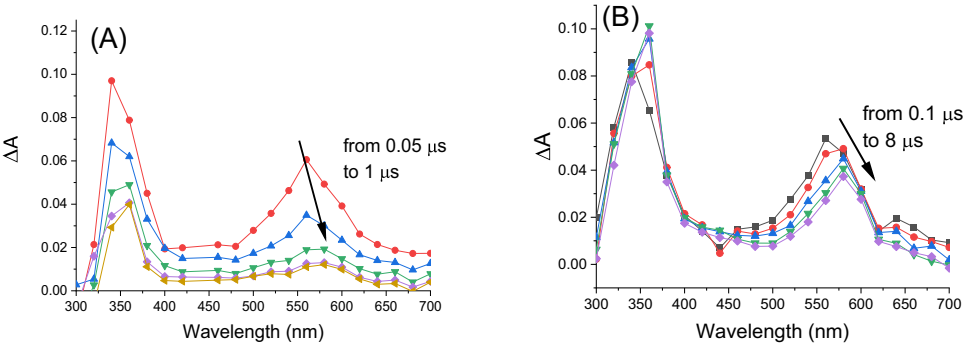

Fig. 8 Transient absorption spectra of CBP in the presence of ε-adduct (2 mM for εdA and 0.3 mM for εdG) in MeCN:H_2O (1:1, v:v) at different times after the 355 nm laser pulse. **A** εdA, **B** εdG

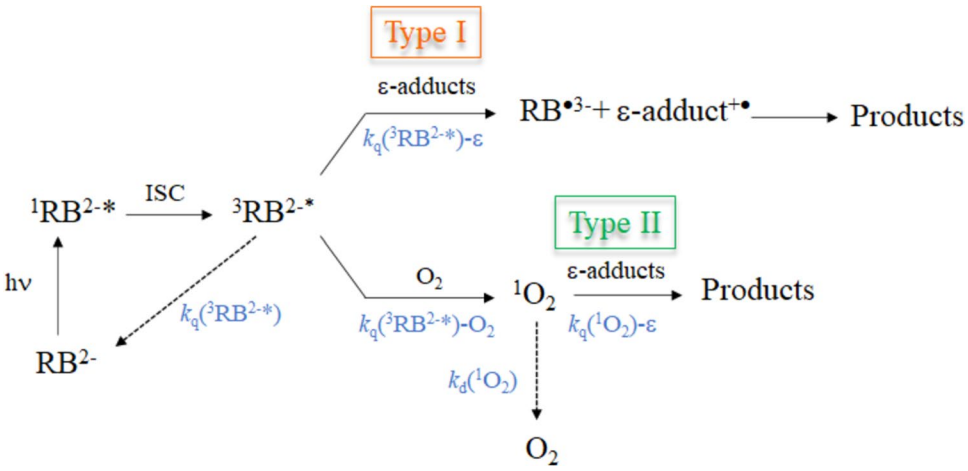

Scheme 2 Deactivation routes intervening in the interaction between excited RB^{2-} and *ε-adducts*

3 Discussion

The photoreactivity of *ε-adducts* triggered by two well-established photosensitizers has been addressed to get mechanistic insight into the processes responsible for their decomposition. In both cases, triplet-mediated processes were observed for the purine adducts.

Firstly, experimental results obtained during irradiation in the presence of RB^{2-} are in agreement with a Type II photosensitization of *ε-adducts*, since the photoreaction takes place more efficiently in deuterated media. However, photophysical studies revealed quenching of $^3RB^{2-}$ triplet excited state by both *ε-adducts*, which opens the way to a potential competition between Type I and Type II oxidation. This process was further investigated to establish the actual mechanism responsible for the *ε-adducts* photodegradation. After RB^{2-} excitation, triplet excited state is efficiently populated ($\phi_{ISC}=0.8$) and then it can be deactivated following different pathways (Scheme 2): (*i*) intrinsic decay, $k_d(^3RB^{2-*})$, (*ii*) quenching by the *ε-adducts*, $k_q(^3RB^{2-*})$-ε, via a Type I process, or (*iii*) quenching by oxygen $k_q(^3RB^{2-*})$-O_2 to form $^1O_2$. This species can be subsequently quenched, $k_q(^1O_2)$-ε, by the ε-adduct to yield a Type II process or can decay naturally to its ground state, $k_d(^1O_2)$.

Table 2 Estimated contributions of the different routes involved in εdA and εdG photosensitization by RB^{2-}

	εdA	εdG
$\%^3RB^{2-*}$ intrinsic decay (Eq. 1)	0.6	0.6
$\%^3RB^{2-*}$ quenching by *ε-adducts* (Eq. 2)	$3{\cdot}10^{-3}$	0.08
$\%^3RB^{2-*}$ quenching by O_2 (Eq. 3)	99.4	99.3
$\%^1O_2$ intrinsic decay (Eq. 4)	99.3	98.9
$\%\ ^1O_2$ quenching by *ε-adducts* (Eq. 5)	0.1	0.5

Contribution of the different routes and of the percentage of Type I vs Type II processes can be estimated by using Eqs. (1–5) [27]. In these equations, $\tau(^3RB^{2-*})$ and $\tau(^1O_2)$ are $^3RB^{2-*}$ and $^1O_2$ lifetimes of ca. 80 and 66 µs, respectively. Values of [ε-adduct] = 20×10^{-6} M and $[O_2]=2.9\times10^{-4}$ M were considered for the concentrations of *ε-adducts* and molecular oxygen in water [28], respectively, and $k_q(^3RB^{2-*})$-O_2 is taken as $7.4\times10^9\ M^{-1}s^{-1}$ [27]. The values of the bimolecular quenching rate constants derived from the laser flash photolysis experiments were considered for $^3RB^{2-*}$ deactivation by εdA and εdG (Table 1).

Equations (1)–(3) allow determining the contribution of the three pathways arising from $^3RB^{2-*}$:

$$\%^3RB^{2-*}\text{Intrinsicdecay}\left(k_{d^3RB^{2-*}}\right)=\frac{\frac{1}{\tau_{3RB^{2-*}}}}{k_{q(^3RB^{2-*})-O_2}\cdot[O_2]+k_{q(^3RB^{2-*})-\varepsilon}\cdot[\varepsilon]+\frac{1}{\tau_{3RB^{2-*}}}}\times100. \quad (1)$$

Type I:

$$\%^3RB^{2-*}\text{Quenching\_}\varepsilon\left(k_{q(^3RB^{2-*})-\varepsilon}\right)=\frac{k_{q(^3RB^{2-*})-\varepsilon}\cdot[\varepsilon]}{k_{q(^3RB^{2-*})-O_2}\cdot[O_2]+k_{q(^3RB^{2-*})-\varepsilon}\cdot[\varepsilon]+\frac{1}{\tau_{3RB^{2-*}}}}\times100. \quad (2)$$

$$\%^1O_2\text{Formation}\left(k_{q(^3RB^{-2*})-O_2}\right)=\frac{k_{q(^3RB^{2-*})-O_2}\cdot[O_2]}{k_{q(^3RB^{2-*})-O_2}\cdot[O_2]+k_{q(^3RB^{2-*})-\varepsilon}\cdot[\varepsilon]+\frac{1}{\tau_{3RB^{2-*}}}}\times100. \quad (3)$$

Next, quenching of $^3RB^{2-*}$ by molecular oxygen can produce $^1O_2$, which could evolve through two further pathways: intrinsic decay (Eq. 4) or quenching by the ε-adduct (at the origin of Type II process, Eq. 5). Therefore, considering

that $^3RB^{2-}$* quenching by O_2 only results in $^1O_2$ formation, Eq. (3), the percentages of these two routes are given by Eqs. (4) and (5):

$$\%^1O_2\text{Intrinsic}_{\text{decay}}\left(\text{kq}^1O_2\right) = \frac{k_{q(^3RB^{2-*})-O_2}\cdot[O_2]}{k_{q(^3RB^{2-*})-O_2}\cdot[O_2]+k_{q(^3RB^{2-*})-\varepsilon}\cdot[\varepsilon]+\frac{1}{\tau_{^3RB^{2-*}}}} x\frac{\frac{1}{\tau^1O_2}}{k_{q(^1O_2)-\varepsilon}\cdot[\varepsilon]+\frac{1}{\tau^1O_2}}\times 100. \quad (4)$$

Type II:

$$\%^1O_2\text{Quenching\_by\_}\varepsilon\left(\text{kq}\left(^1O_2\right)-\varepsilon\right) = \frac{k_{q(^3RB^{2-*})-O_2}\cdot[O_2]}{k_{q(^3RB^{2-*})-O_2}\cdot[O_2]+k_{q(^3RB^{2-*})-\varepsilon}\cdot[\varepsilon]+\frac{1}{\tau_{^3RB^{2-*}}}} x\frac{k_{q(^1O_2)-\varepsilon}\cdot[\varepsilon]}{k_{q(^1O_2)-\varepsilon}\cdot[\varepsilon]+\frac{1}{\tau^1O_2}}\times 100. \quad (5)$$

The contributions of the different pathways for εdA and εdG photosensitization by RB^{2-} are summarized in Table 2

It is clearly observed that the main deactivation pathway of $^3RB^{2-}$* under aerobic conditions consists in its quenching by molecular oxygen, leading mainly to $^1O_2$ formation (Eq. 3), which accounts for 99.4% and 99.3% for εdA and εdG, respectively. Nevertheless, subsequent quenching of $^1O_2$ by the lesions occurs with relatively low bimolecular rate constants, $k_q(^1O_2)$-ε of ca. 9.5×10^5, 3.6×10^6 $M^{-1}s^{-1}$ for εdA and εdG, respectively. Thus, at the lesion concentration of 20 μM, almost all the $^1O_2$ decays without reacting ($\%^1O_2$ intrinsic decay Eq. 4, Table 2). Nevertheless, under aerobic conditions, the contribution of a Type II process is higher than that of the Type I pathway (Table 2).

This conclusion can be directly drawn for εdG, as it has been previously established that this lesion is able to react with $^1O_2$, cleanly generated from thermal degradation of naphthalene-derived endoperoxides, to regenerate the original dG [17]. In the present work, the similarity of the results between εdA and εdG also points to an analogous reactivity with $^1O_2$.

However, a Type I pathway is conceivable in the case of these purine adducts, but depends on the photoredox properties of the photosensitizer. As a matter of fact, the bimolecular quenching rate constants of $^3RB^{2-}$* by the lesions are at least two order of magnitude lower than those determined for ^{3}CBP*, which is a better photooxidant.

To further investigate the Type I route, experiments were run under anaerobic conditions using CBP as photosensitizer. In line with that reactivity, for both *ε-adducts* a clear electron transfer was evidenced by the formation of $CBPH^{\bullet}$ (Fig. 8). Although the reduction potential value for εdG has not been reported, it appears from our experiments that, like the corresponding canonical nucleobase dG, it might be more easily oxidized than εdA. This assumption is not only based on $CBPH^{\bullet}$ detection, but also on the fact that the highest quenching rate constants were determined for $^3RB^{2-}$* and ^{3}CBP* by this lesion (Table 1).

On the basis of these results, mechanisms could be proposed for Type I and Type II photosensitization of *ε-adducts* (Scheme 1). Electron transfer from εdG to ^{3}CBP*, or $^3RB^{2-}$*, could result in the formation of cation radical **I** centered on the etheno ring, which after nucleophilic addition of water and deprotonation yields radical **II**. This radical can further react with water to yield glycol intermediate **III**, or disproportionate and after addition of water can also give rise to **III**. Then, dG is formed after attack of water and loss of formic acid. A similar mechanism is proposed for dA formation from εdA. In the case of $^1O_2$-mediated process, its addition on the εdG double bond of the etheno ring leads, as proposed by Martinez et al.[17], to an unstable dioxetane **IV** that cleaves to form intermediates **III** or **V**. For intermediate **III**, the following reaction steps are then similar to those described for Type I. For intermediate **V**, compounds **VIa** or **VIb** are formed after attack of water, and loss of formic acid; these intermediates after a second addition of water and elimination of a second molecule of formic acid lead to the regenerated base dG.

4 Conclusions

As a general outcome, the photolability of *ε-adducts* under photosensitization conditions was studied. The use of photosensitizers acting by Type I and/or Type II mechanisms has shown that *ε-adducts* are sensitive to both types of processes. Interestingly, both oxidation processes lead to photoproducts that correspond to the repaired nucleosides. Despite that recovery of the original bases is not quantitative and that other unidentified photoproducts are formed, the obtained results reveal that photosensitization might be proposed as a new strategy of photorepair for *ε-adducts*.

5 Experimental section

5.1 Chemicals

The 2′-deoxynucleosides dA and dG were purchased from Merck. εdA was from Carbosynth Biosynth, and εdG was synthesized as previously described [14].

5.2 UV–Vis spectrometry

All UV–Vis absorption spectra were registered with a single beam Varian Cary 60 spectrophotometer, using quartz cells of 1cm optical path length.

5.3 Phosphorescence spectroscopy

RB^{2-} phosphorescence was recorded at room temperature using a customized setup having a diode-pumped Nd:YAG laser as a light source (FTSS355-Q3 model from CryLas, Germany), which was tuned to its second harmonic (532 nm). The detection system consists of a monochromator (CM110) from Spectral Product and a PMT from Hamamatsu (H11526-110-NN detection range 230 nm-700 nm); the PMT output is sent to a multi-channel scaler (TimeHarp 260-Nano, PicoQuant). All solutions were prepared in ethanol, adjusting their absorbance at ca. 0.5 of the excitation wavelength (with a cuvette of 1 cm optical pathway).

5.4 Direct detection of singlet oxygen luminescence

Time-resolved near-infrared (TRNIR) phosphorescence detection of $^1O_2$ at 1270 nm was carried out using a customized setup. A diode-pumped Nd:YAG laser (FTSS355-Q3, CryLas, Germany), tuned to its second harmonic (532 nm) and working at a repetition rate of 1 kHz, was used as an excitation source for RB^{2-}. The kinetic traces were collected by isolating the 1270 nm intrinsic phosphorescence of $^1O_2$ using a monochromator (Digikröm CM110 1/8 m, Spectral Products, Putnam, CT) equipped with a 1150 nm cut-on long-pass filter (FEL1150, ThorLabs, Newton, NJ) and a 1064 nm notch filter (NF1064-44, ThorLabs) mounted side by side at its entry port and directed to a TE-cooled photomultiplier tube (PMT, H10330A-45, Hamamatsu, Japan), working at -908 V and operated in the photon-counting mode.

After amplification by a 1.1 GHz preamplifier module (PAM-102-T, PicoQuant GmbH, Germany), the output of the PMT was sent to a multi-channel scaler (TimeHarp 260-Nano, PicoQuant). The signals were collected in D_2O for 300 s with 256 ns resolution. The kinetic traces were least-square fitted to the following equation using Prism 7.0 (GraphPad Software Inc., La Jolla, CA) with τ_Δ, τ_T, and S_0 as free parameters. The quality of the fittings was assessed by the residual plots.

$$S(t) = S_0 \frac{\tau_\Delta}{(\tau_\Delta - \tau_T)} \left(\exp\left(\frac{-t}{\tau_\Delta}\right) - \exp\left(\frac{-t}{\tau_T}\right) \right), \quad (6)$$

where S(t) is the signal intensity at a time t, $\tau\Delta$ is the $^1O_2$ lifetime and ,τ_T is the photosensitizer's triplet state lifetime. S_0 is defined as the concentration of $^1O_2$ being produced in a given system.

5.5 Steady-state photolysis

Irradiation of the samples containing RB^{2-} was performed under anaerobic and aerobic conditions in Pyrex vials using a Luzchem photoreactor (model LZV-4V) with 8 FLS T5 8W840/CW fluorescent lamps (emission range 350–700 nm). For CBZ, the samples were irradiated under anaerobic conditions in quartz cuvettes using a Luzchem photoreactor equipped with UVA-BLB lamps (maximum output at 365 nm).

5.6 Laser flash photolysis

Laser flash photolysis experiments were performed by exciting at 355 and 532 nm, using the third and second harmonic, respectively, of a pulsed laser Nd:YAG (L52137V LOTIS TII) with a pulse duration of ca. 10 ns. The full system comprises a pulsed laser, a xenon lamp (Lo 255 Oriel), a monochromator (Oriel 77,200), a photomultiplier (Oriel 70,705) and an oscilloscope (TDS-640A Tektronic). The output signal from the oscilloscope was transferred to a personal computer.

All experiments were performed in a quartz cell of 1 cm optical path length. Compounds' concentration was adjusted to have an absorbance of ca. 0.3 at the excitation wavelength. Before running the measurements under anaerobic conditions, solutions were flushed with N_2, for 15 min. Laser energies ranging 20 mJ per pulse were used.

5.7 HPLC analysis

All irradiation mixtures were analyzed on an Agilent 1100 Series HPLC setup equipped with a diode-array detector covering a detection range from 200 to 400 nm. Analyses were performed using a Zorbax Eclipse Plus C18 (100×4.6 mm, 3.5 µm) column (ZC), with a detection fixed at 260 nm. For εdG photosensitization, the analysis was run under isocratic conditions for 25 min with a mobile phase of 5% acetonitrile and 95% H_2O acidified with trifluoroacetic acid at pH ca. 3, then a gradient was applied to reach 95% of acetonitrile in 10 min, and these conditions were maintained for 10 min; the flow rate was set at 0.3 mL/min. For εdA photosensitization, the analysis was run under isocratic conditions for 17 min with a mobile phase of 3% acetonitrile and 97% H_2O acidified with trifluoroacetic acid at pH ca. 3, then a gradient was applied to reach 95% of acetonitrile in 10 min, and these conditions were maintained for 10 min; the flow rate was set at 0.4 mL/min. The yields of photorepair

and concentration of repaired and damage nucleosides were determined from calibration curves using pure compounds.

Mass analyses were performed on a system composed of Shimadzu modules: a DGU-405 degassing unit, an LC-40D xs solvent delivery module, an SCL-40system controller, SIL-40C xs autosampler, a CTO-40C column oven, an SPD-M40 Photodiode array detector, and a Triple Quadrupole Mass Spectrometer LC 840 model. The same column (Zorbax Eclipse Plus C18) and eluting conditions (with the only difference being that solvents were acidified with HCOOH) as described above were used. Analysis was performed using electrospray in positive mode with a capillary voltage of 4.5 kV. The following MS parameters were used in the analysis: nebulizing gas flow: 3 L min^{-1}, drying gas flow: 15 L min^{-1}, interface temperature: 350 ºC, desolvation line temperature: 250 ºC, and heating block: 400 ºC. The data were processed using Lab Solutions software.

Supplementary Information The online version contains supplementary material available at https://doi.org/10.1007/s43630-024-00663-x.

Acknowledgements Financial support from the Spanish (projects PID2021-128348NB-I00 and Severo Ochoa Center of Excellence Program CEX2021-001230-S, funded by MCIN/AEI/https://doi.org/10.13039/501100011033/and "FEDER a way of making Europe", and grant BES-2016-077517 to P. L.-A.) and regional (CIAICO/2021/061) governments is acknowledged.

Funding Open Access funding provided thanks to the CRUE-CSIC agreement with Springer Nature.

Data availability The data that support the findings of this study are available in the supplementary information of this article.

Declarations

Conflict of interest The authors declare no competing financial interests.

Open Access This article is licensed under a Creative Commons Attribution 4.0 International License, which permits use, sharing, adaptation, distribution and reproduction in any medium or format, as long as you give appropriate credit to the original author(s) and the source, provide a link to the Creative Commons licence, and indicate if changes were made. The images or other third party material in this article are included in the article's Creative Commons licence, unless indicated otherwise in a credit line to the material. If material is not included in the article's Creative Commons licence and your intended use is not permitted by statutory regulation or exceeds the permitted use, you will need to obtain permission directly from the copyright holder. To view a copy of this licence, visit http://creativecommons.org/licenses/by/4.0/.

References

1. (2021). DNA Photodamage. From Light absorption to cellular response and skin cancer. In: Improta, R., Douki, T., Eds. *Comprehens*. Royal Society of Chemistry.
2. Di Mascio, P., Hamblin, M. R., Thomas, A. H., Vignoni, M., Lorente, C., Ghogare, A. A., Nunez, S. C., Cadet, J., Baptista, M. S., Ribeiro, M. S., Greer, A., Yoshimura, T. M., Cadet, J., Di Mascio, P., Ghogare, A. A., Greer, A., Hamblin, M. R., Lorente, C., Nunez, S. C., … Yoshimura, T. M. (2017). Type I and type II photosensitized oxidation reactions: guidelines and mechanistic pathways. *Photochemistry and Photobiology, 93*(4), 912–919. https://doi.org/10.1111/php.12716
3. Cadet, J., Douki, T., & Ravanat, J.-L. (2008). Oxidatively Generated Damage to the Guanine Moiety of DNA: Mechanistic Aspects and Formation in Cells. *Accounts of Chemical Research, 41*(8), 1075–1083. https://doi.org/10.1021/ar700245e
4. Ravanat, J. L., Saint-Pierre, C., & Cadet, J. (2003). One-electron oxidation of the guanine moiety of 2′-deoxyguanosine: Influence of 8-oxo-7,8-dihydro-2′-deoxyguanosine. *Journal of the American Chemical Society, 125*(8), 2030–2031. https://doi.org/10.1021/ja028608q
5. Cui, L., Ye, W., Prestwich, E. G., Wishnok, J. S., Taghizadeh, K., Dedon, P. C., & Tannenbaum, S. R. (2013). Comparative analysis of four oxidized guanine lesions from reactions of DNA with peroxynitrite, singlet oxygen, and γ-radiation. *Chemical Research in Toxicology, 26*(2), 195–202. https://doi.org/10.1021/tx300294d
6. Kino, K., Takao, M., Miyazawa, H., & Hanaoka, F. (2012). A DNA oligomer containing 2,2,4-Triamino-5(2H)-oxazolone is incised by human NEIL1 and NTH1. *Mutation Research and Molecular Mechanisms of Mutagenesis, 734*(1–2), 73–77. https://doi.org/10.1016/J.MRFMMM.2012.03.007
7. Hori, M., Suzuki, T., Minakawa, N., Matsuda, A., Harashima, H., & Kamiya, H. (2011). Mutagenicity of secondary oxidation products of 8-Oxo-7,8-Dihydro-2′-Deoxyguanosine 5′-Triphosphate (8-Hydroxy-2′- Deoxyguanosine 5′-Triphosphate). *Mutation Research and Molecular Mechanisms of Mutagenesis, 714*(1–2), 11–16. https://doi.org/10.1016/J.MRFMMM.2011.05.015
8. Tudek, B., Zdżalik-Bielecka, D., Tudek, A., Kosicki, K., Fabisiewicz, A., & Speina, E. (2017). Lipid peroxidation in face of DNA damage, DNA repair and other cellular processes. *Free Radical Biology & Medicine, 107*, 77–89. https://doi.org/10.1016/j.freeradbiomed.2016.11.043
9. El Ghissassi, F., Barbin, A., Nair, J., & Bartsch, H. (1995). Formation of 1, N6-ethenoadenine and 3, N4-ethenocytosine by lipid peroxidation products and nucleic acid bases. *Chemical Research in Toxicology, 8*, 278–283. https://doi.org/10.1021/tx00044a013
10. Basu, A. K., Wood, M. L., Niedernhofer, L. J., Ramos, L. A., & Essigmann, J. M. (1993). Mutagenic and genotoxic effects of three vinyl chloride-induced DNA lesions: 1, N6-ethenoadenine, 3, N4-ethenocytosine, and 4-Amino-5-(Imidazol-2-Yl)Imidazole. *Biochemistry, 32*, 12793–12801. https://doi.org/10.1021/bi00210a031
11. Chung, F.-L., Chen, H.-J.C., & Nath, R. G. (1996). Lipid Peroxidation as a potential endogenous source for the formation of exocyclic DNA adducts. *Carcinogenesis, 17*(10), 2105–2111. https://doi.org/10.1093/carcin/17.10.2105
12. Fernando, R. C., Nair, J., Barbin, A., Miller, J. A., & Bartsch, H. (1996). Detection of 1, N6-ethenodeoxyadenosine and 3, N4-ethenodeoxycytidine by immunoaffinity/ 32 P-post-labelling in liver and lung DNA of mice treated with ethylcarbamate (Urethane) or its metabolites. *Carcinogenesis, 17*(8), 1711–1718. https://doi.org/10.1093/carcin/17.8.1711
13. Yu, Y., Cui, Y., Niedernhofer, L. J., & Wang, Y. (2016). Occurrence, biological consequences, and human health relevance of oxidative stress-induced DNA damage. *Chemical Research in Toxicology, 29*(12), 2008–2039. https://doi.org/10.1021/acs.chemrestox.6b00265
14. Lizondo-Aranda, P., Gustavsson, T., Martínez-Fernández, L., Improta, R., & Lhiaubet-Vallet, V. (2024). The excited state

dynamics of a mutagenic guanosine etheno adduct investigated by femtosecond fluorescence spectroscopy and quantum mechanical calculations. *Chemistry-A European Journal.* https://doi.org/10.1002/chem.202401835. just accep.

15. Lizondo-Aranda, P., Martínez-Fernández, L., Miranda, M. A., Improta, R., Gustavsson, T., & Lhiaubet-Vallet, V. (2022). The excited state dynamics of a mutagenic cytidine etheno adduct investigated by combining time-resolved spectroscopy and quantum mechanical calculations. *Journal of Physical Chemistry Letters, 13*(1), 251–257. https://doi.org/10.1021/acs.jpclett.1c03534
16. Barbati, S., Bonnefoy, A., Botta, A., & Chiron, S. (2010). Secondary oxidation of cyclic 1, N2-propano and 1, N2-etheno-2′-deoxyguanosine DNA adducts. Consequences in oxidative stress biomarker development. *Chemosphere, 80*(9), 1081–1087. https://doi.org/10.1016/J.CHEMOSPHERE.2010.04.075
17. Martinez, G. R., Brum, H., Sassaki, G. L., De Souza, L. M., Loureiro, A. P. D. M., De Medeiros, M. H. G., & Di Mascio, P. (2018). Oxidation of 1-N 2-etheno-2′-deoxyguanosine by singlet molecular oxygen results in 2′-deoxyguanosine: A pathway to remove exocyclic DNA damage? *Biological Chemistry, 399*(8), 859–867. https://doi.org/10.1515/hsz-2017-0337
18. Ludvíková, L., Friš, P., Heger, D., Šebej, P., Wirz, J., & Klán, P. (2016). Photochemistry of rose Bengal in water and acetonitrile: A comprehensive kinetic analysis. *Physical Chemistry Chemical Physics: PCCP, 18*(24), 16266–16273. https://doi.org/10.1039/C6CP01710J
19. Lambert, C. R., & Kochevar, I. E. (1997). Electron transfer quenching of the rose Bengal triplet state. *Photochemistry and Photobiology, 66*(1), 15–25. https://doi.org/10.1111/J.1751-1097.1997.TB03133.X
20. Cuquerella, M. C., Lhiaubet-Vallet, V., Cadet, J., & Miranda, M. A. (2012). Benzophenone photosensitized DNA damage. *Accounts of Chemical Research, 45*(9), 1558–1570. https://doi.org/10.1021/ar300054e
21. Cuquerella, M. C., Lhiaubet-Vallet, V., Bosca, F., & Miranda, M. A. (2011). Photosensitised pyrimidine dimerisation in DNA. *Chemical Science, 2*, 1219–1232. https://doi.org/10.1039/c1sc00088h
22. Ogilby, P. R., & Foote, C. S. (1983). Chemistry of singlet oxygen. 42. Effect of solvent, solvent isotopic substitution, and temperature on the lifetime of singlet molecular oxygen (1.DELTA.G). *Journal of the American Chemical Society, 105*(11), 3423–3430. https://doi.org/10.1021/ja00349a007
23. Ravanat, J. L., & Dumont, E. (2022). Reactivity of Singlet Oxygen with DNA, an Update†. *Photochemistry and Photobiology, 98*(3), 564–571. https://doi.org/10.1111/PHP.13581
24. Lambert, C. R., & Kochevar, I. E. (1996). Does rose Bengal triplet generate superoxide anion? *Journal of the American Chemical Society, 118*(13), 3297–3298. https://doi.org/10.1021/ja9600800
25. Islam, S. D. M., & Ito, O. (1999). Solvent effects on rates of photochemical reactions of rose bengal triplet state studied by nanosecond laser photolysis. *Journal of Photochemistry and Photobiology, A: Chemistry, 123*(1–3), 53–59. https://doi.org/10.1016/S1010-6030(99)00042-8
26. Lineros-Rosa, M., Miranda, M. A., & Lhiaubet-Vallet, V. (2020). A sunscreen-based photocage for carbonyl groups. *Chemistry–A European Journal, 26*(32), 7205–7211. https://doi.org/10.1002/CHEM.202000123
27. Martinez-Haya, R., Miranda, M. A., & Marin, M. L. (2018). Type I vs Type II photodegradation of pollutants. *Catalysis Today, 313*, 161–166. https://doi.org/10.1016/J.CATTOD.2017.10.034
28. Montalti, M., Credi, A., Prodi, L., & Gandolfi, M. T. (2006). *Handbook of photochemistry* (3rd ed.). Taylor & Francis Group.